

Spin-crossover tuning of the luminescence in 2D Hofmann-type compounds in bulk and exfoliated flakes

Víctor García-López,^{a,†} Francisco Marques-Moros,^{a,†} José Troya,^a Josep Canet-Ferrer,^{*a} Miguel Clemente-León^{*a} and Eugenio Coronado^a

^a Instituto de Ciencia Molecular (ICMol), Universitat de València, C/ Catedrático José Beltrán 2, 46980 Paterna, Spain. Fax: 34 963543273; Tel: 34 963544419; E-mail: miquel.clemente@uv.es, jose.canet-ferrer@uv.es.

† V. G.-L. and F. M.-M. contributed equally to this work.

Supporting information

Table of contents

Experimental section

Table S1. Crystallographic table

Fig. S1. Simulated (blue) and experimental (red) PXRD pattern of **2**.

Fig. S2 *ab* (left) and *bc* (right) plane projections of the **1·Zn** (C (black), N (blue), O (red), Zn (gray), Pt (dark blue)).

Fig. S3. Simulated (continued line) and experimental (dashed line) PXRD of **1**.

Fig. S4 $\chi_M T$ vs temperature of a freshly filtered sample of **1**.

Fig. S5 PL dependence on the temperature for bulk crystals of a) **1**, b) **2**, c) **1·Zn**, and d) **2·Zn**.

Fig. S6 Dependence of integrated PL intensity (area) vs temperature for **2**.

Fig. S7 Stack of temperature-dependent Raman spectra of **1** in bulk in the range between 1290 and 1660 cm^{-1} .

Fig. S8 Example of optical microscopy images of compound **1** after Scotch tape exfoliation.

Fig. S9 Example of optical microscopy images of compound **2** after Scotch tape exfoliation.

Fig. S10 Optical microscopy and AFM images of **2**. General optical image (left). AFM image (bottom left) of the selected region in dashed white left image with its corresponding height profile (top right; marked in dashed blue in the bottom right image).

Fig. S11 Top panel). Raman fingerprints of **2** (green) and an exfoliated flake of 116 nm thickness (blue) in the 200–2300 cm^{-1} range at RT. (Bot panel). Optical and AFM images of the exfoliated flake of **2** after Raman measurement. General optical image (top right). AFM image (left) of the selected region in dashed white in the top right image and its height profile (bottom right; marked in dashed blue in the left image).

Fig. S12 PL power dependence of a bulk crystal of **1** at room temperature. a) Recorded spectra at the different 375 nm excitation powers. b) Result of the Integrated Area of the PL band for the different powers measured in a).

Fig. S13 Resonant PL dependence on the temperature for a) **2** and b) **1** exfoliated flakes. A grey dashed line has been added for reference to the eye.

Fig. S14 PL Lorentzian peak deconvolution at different temperatures of an exfoliated sample of **1**. Representative temperatures below and above the SCO transition have been chosen.

Fig. S15 Results of the Lorentzian peak deconvolution for the exfoliated sample of **1**. a) Displays the Central wavelength, b) the FWHM and c) the Integrated Area of the 3 Lorentzian peaks deconvolution the PL spectra shown in **Fig. S11**.

Fig. S16 Raman shift of the CN vibration with the temperature of a) **2** flakes, and b) bulk **1·Zn** sample. The plot at the left represents the central frequency of the identified Raman vibrational bands. The stack of Raman spectra is shown at the right, which y-axis accounts for intensity in arbitrary units.

Fig. S17 Stack of temperature-dependent Raman spectra of **1** flakes in the 1350.2220 cm^{-1} range.

Experimental section

All chemicals are commercially available and were used as received without further purification.

Caution! Perchlorate salts are explosive when subjected to heat or friction, they must be handled with care.

Synthesis of furanylidene-4H-1,2,4-triazol-4-amine (furtrz)

2-furfural (2.06 g, 28.5 mmol) and 4-amino-1,2,4-triazole (2g, 23.7 mmol) were dissolved in 50 mL of ethanol together with 2 drops of sulfuric acid. The mixture was kept under reflux for 5h. After cooling down, a precipitate appears. It was filtered and washed with water and ethanol. Then, it was dissolved in 50mL of MeCN and filtered over SiO₂. A white powder was obtained after recrystallization in ethanol. ¹H NMR

Synthesis of [Fe^{II}(furtrz)₂(Pt(CN)₄)]·4(H₂O) (1)

Fe(ClO₄)₂·xH₂O (43.44 mg, 0.12 mmol) and furtrz (38,88 mg, 0.24 mmol) in 3mL of 1:1 water/EtOH were carefully layered on top of K₂[Pt(CN)₄]₂ (44 mg, 0.12 mmol) in 3mL of water. After a week, Yellowish plates of **1** suitable for single-crystal X-ray diffraction analysis were obtained. The crystals were filtered and washed with abundant water. Anal. Calcd for FePt(N₄C₇H₆O)₂(CN)₄(H₂O)₃: C, 29.40; H, 2.74; N, 22.86 %. Found: C, 29.20; H, 2.53; N, 22.86 %.

Synthesis of (E)-2-(((4H-1,2,4-triazol-4-yl)imino)methyl)phenol (saltrz)

Salicylaldehyde (1.221 g, 10 mmol) was dissolved in 20mL of ethanol and added to a solution of 4-amino-4H-1,2,4-triazole (0.841g, 10 mmol) in 20mL of the same solvent. After stirring for 30 min, the mixture was kept in reflux over 1 h. After cooling down, crystals of saltrz were obtained. ¹H NMR

Synthesis of [Fe₃(saltrz)₆(Pt(CN)₄)₃]·8(H₂O) (2) and [Zn₃(saltrz)₆(Pt(CN)₄)₃]·8(H₂O) (2·Zn)

0.12 mmol of Fe(ClO₄)₂·xH₂O (**2**) or Zn(ClO₄)₂·xH₂O (**2·Zn**) and saltrz (45.60 mg, 0.24 mmol) in 3mL of 1:1 water/EtOH were carefully layered on top of K₂[Pt(CN)₄]₂ (48 mg, 0.12 mmol) in 3mL of water. After a week, Yellowish plates of **2** were obtained. The crystals were filtered and washed with abundant water. Anal. Calcd for Fe(C₇H₇N₄O)₂Pt(CN)₄(CH₃CH₂OH)(H₂O): C, 32.23; H, 2.98; N, 22.55 %. Found: C, 29.20; H, 2.53; N, 22.86 %. Anal. Calcd for FePt(N₄C₇H₆O)₂(CN)₄(H₂O)(H₂O)₂: C, 29.40; H, 2.74; N, 22.86 %. Found: C, 29.20; H, 2.53; N, 22.86 %.

Synthesis of [Zn^{II}(furtrz)₂(Pt(CN)₄)]·4(H₂O) (1·Zn)

Zn(ClO₄)₂·xH₂O (44.7 mg, 0.12 mmol) and furtrz (38,88 mg, 0.24 mmol) in 3mL of 1:1 water/EtOH were carefully layered on top of K₂[Pt(CN)₄]₂ (44 mg, 0.12 mmol) in 3mL of water. After a week, white plates suitable for single-crystal X-ray diffraction analysis were obtained. The crystals were filtered and washed with abundant water.

Table S1. Crystallographic table

Compound	1	1	1	1·Zn	2·Zn
Empirical formula	C ₁₈ H ₂₃ FeN ₁₂ O ₆ Pt	C ₁₈ H ₂₃ FeN ₁₂ O ₆ Pt	C ₁₈ H ₂₃ FeN ₁₂ O ₆ Pt	C ₂₀ H ₁₄ N ₁₂ O ₄ PtZn	C ₆₆ H ₆₄ N ₃₆ O ₁₄ Pt ₃ Zn ₃
Formula weight	754.42	754.42	754.42	746.89	2366.91
Temperature/K	120.00(10)	204.00(10)	240.00(10)	119.99(10)	120.0
Crystal color	Red	Orange	Yellowish	White	White
Crystal system	orthorhombic	orthorhombic	orthorhombic	monoclinic	triclinic
Space group	Pnma	Pnma	Pnma	P2 ₁ /c	P-1
a/Å	14.1132(4)	14.250(2)	14.3777(16)	7.42223(4)	10.5209(2)
b/Å	7.1602(2)	7.3249(14)	7.5227(7)	23.62028(13)	13.7504(3)
c/Å	23.5105(7)	23.717(5)	23.891(2)	14.43772(8)	16.3718(2)
α/°	90	90	90	90	108.026(2)
β/°	90	90	90	90.6042(5)	107.8650(10)
γ/°	90	90	90	90	95.6690(10)
Volume/Å ³	2375.81(12)	2475.6(8)	2584.0(5)	2531.01(2)	2093.93(7)
Z	4	4	4	4	1
ρ _{calc} /cm ³	2.109	1.831	1.754	1.960	1.877
μ/mm ⁻¹	6.556	6.270	6.007	11.820	10.771
F(000)	1468.0	1308.0	1308.0	1432.0	1148.0
Crystal size/mm ³	0.15 × 0.1 × 0.03	0.12 × 0.12 × 0.03	0.15 × 0.1 × 0.03	0.211 × 0.108 × 0.057	0.05 × 0.03 × 0.02
Radiation	MoKα (λ = 0.71073)	MoKα (λ = 0.71073)	MoKα (λ = 0.71073)	CuKα (λ = 1.54184)	CuKα (λ = 1.54184)
2θ range for data collection/°	6.612 to 56.088	6.672 to 59.954	6.614 to 55.902	7.176 to 157.558	6.076 to 156.872
Index ranges	-18 ≤ h ≤ 17, -8 ≤ k ≤ 8, -31 ≤ l ≤ 29	-20 ≤ h ≤ 17, -6 ≤ k ≤ 10, -22 ≤ l ≤ 32	-17 ≤ h ≤ 17, -8 ≤ k ≤ 9, -29 ≤ l ≤ 29	-7 ≤ h ≤ 9, -30 ≤ k ≤ 29, -18 ≤ l ≤ 17	-11 ≤ h ≤ 13, -17 ≤ k ≤ 17, -20 ≤ l ≤ 20
Reflections collected	9019	11639	14380	54366	41269
Independent reflections	2735 [R _{int} = 0.0844, R _{sigma} = 0.1021]	3473 [R _{int} = 0.0958, R _{sigma} = 0.1039]	3015 [R _{int} = 0.1491, R _{sigma} = 0.1485]	5440 [R _{int} = 0.0597, R _{sigma} = 0.0255]	8751 [R _{int} = 0.0485, R _{sigma} = 0.0344]
Data/restraints/parameters	2735/127/259	3473/132/232	3015/133/220	5440/3/345	8751/0/566
Goodness-of-fit on F ²	1.090	1.107	1.107	1.058	1.178
Final R indexes [I >= 2σ (I)]	R ₁ = 0.0555, wR ₂ = 0.1135	R ₁ = 0.0837, wR ₂ = 0.1886	R ₁ = 0.1249, wR ₂ = 0.3085	R ₁ = 0.0266, wR ₂ = 0.0649	R ₁ = 0.0305, wR ₂ = 0.0780
Final R indexes [all data]	R ₁ = 0.0897, wR ₂ = 0.1358	R ₁ = 0.1060, wR ₂ = 0.2052	R ₁ = 0.1688, wR ₂ = 0.3313	R ₁ = 0.0273, wR ₂ = 0.0654	R ₁ = 0.0345, wR ₂ = 0.0807
Largest diff. peak/hole / e Å ⁻³	3.66/-2.80	6.80/-2.65	11.99/-7.98	1.42/-1.24	1.95/-1.28

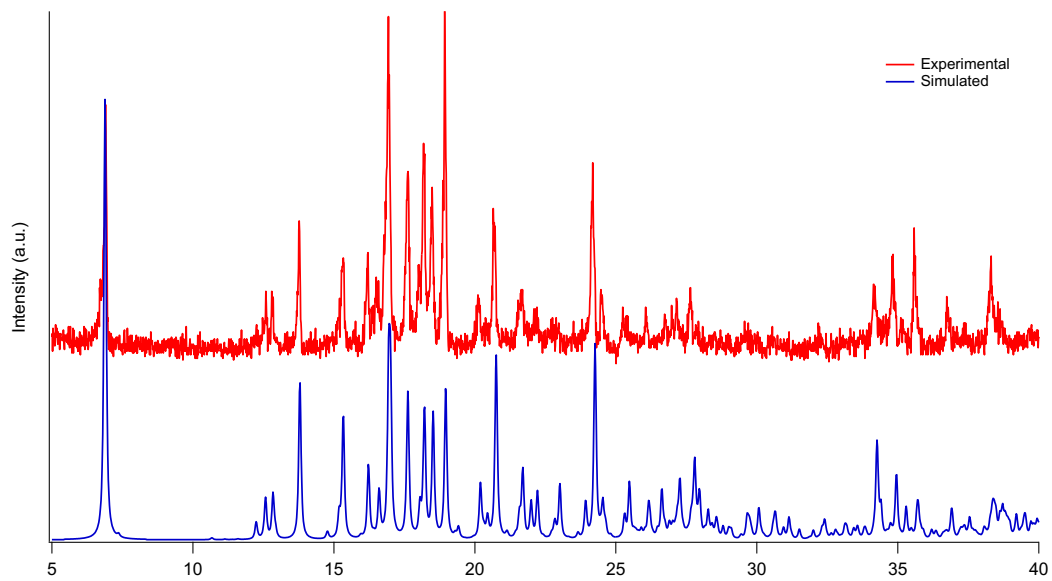


Fig. S1. Simulated (blue) and experimental (red) PXRD pattern of **2**.

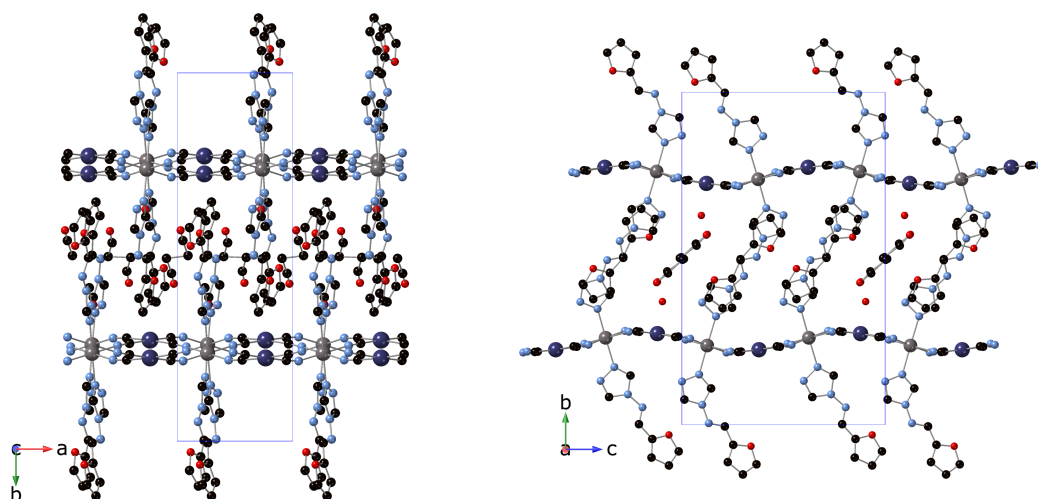


Fig. S2 *ab* (left) and *bc* (right) plane projections of the **1·Zn** (C (black), N (blue), O (red), Zn (gray), Pt (dark blue)). Hydrogen atoms have been omitted for clarity.

Single crystal X-ray structure analysis of the Zn reference compound $[\text{Zn}(\text{furtrz})_2[\text{Pt}(\text{CN})_4]] \cdot \text{EtOH} \cdot \text{H}_2\text{O}$ (**1·Zn**) was performed at 120 K. It crystallizes in the monoclinic $P2_1/c$ space group in contrast to orthorhombic $Pnma$ space group of the iron compound **1**. The asymmetric unit contains crystallographically independent Zn, Pt and two furtrz with occupancies of 1 plus four CN^- ligands and one water molecule plus a disordered EtOH molecule. Therefore, a different solvate to that of **1**, which contains four H_2O molecules per Fe atom, is obtained. It presents the typical structure of 2D Hofmann materials formed by layers of Zn^{2+} centers connected to four equivalent square planar N-donor $[\text{Pt}(\text{CN})_4]^{2-}$ in the equatorial positions and to two N from triazole of two furtrz ligands in the axial positions completing the octahedral coordination. Thus, 2D undulating layers of composition $\text{Zn}[\text{Pt}(\text{CN})_4]_n$ are generated along the *ac* plane with furtrz ligands protruding above and below the layer (see **Fig. S2**). The inter-digitation of the furtrz ligands allows an efficient packing of the layers with enough space to host solvent water molecules, giving an overall formula of $[\text{Zn}(\text{furtrz})_2[\text{Pt}(\text{CN})_4]] \cdot \text{EtOH} \cdot \text{H}_2\text{O}$. Due to the undulation of the framework, furtrz ligands coming from different layers assembly in pairs with neighboring furtrz along the *a* axis.

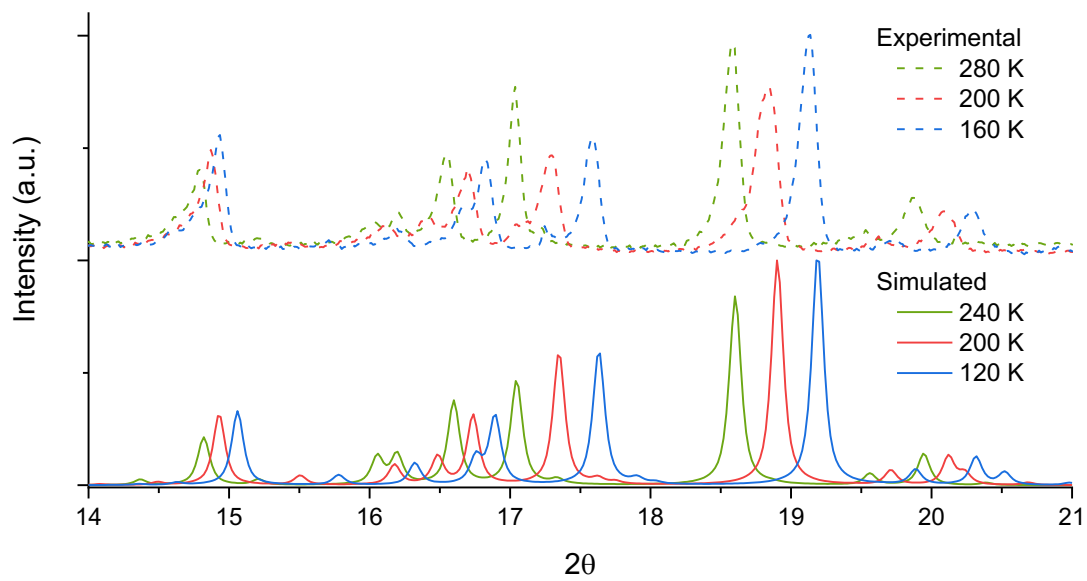


Fig. S3. Simulated (continued line) and experimental (dashed line) PXR D of **1**.

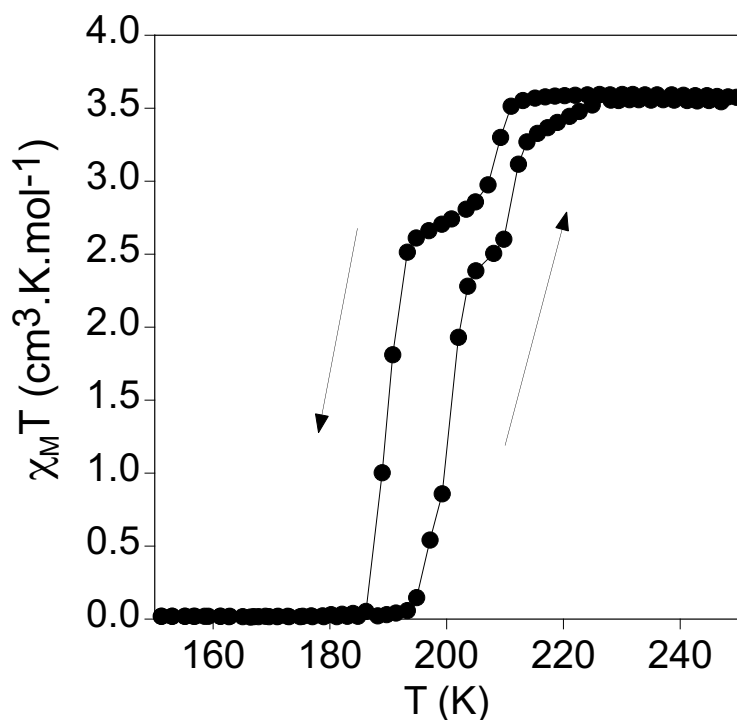


Fig. S4 $\chi_M T$ vs temperature of a freshly filtered sample of **1**.

The thermal dependence of the product of the molar magnetic susceptibility with temperature ($\chi_M T$) of a freshly filtered sample of **1** is shown in Fig. S4. In the cooling mode, $\chi_M T$ value remains constant at ca. 3.6 emu·K·mol⁻¹ from 300 to 210 K, which is the expected value for a Fe(II) HS. At lower temperatures, it shows an abrupt decrease in two steps. In the first one, $\chi_M T$ decreases from 3.5 emu·K·mol⁻¹ at 210 K to 2.9 emu·K·mol⁻¹ at 205 K, which represents the conversion of 1/4 of the Fe(II) sites from the HS to the LS. This is followed by a plateau from which a gradual decrease to 2.6 emu·K·mol⁻¹ at 195 K takes place. At lower temperatures, there is the second abrupt decrease to reach values close to 0 emu·K·mol⁻¹ at 185 K corresponding to a complete spin conversion. In the warming mode, the same two-step spin transition is maintained with small hysteresis loops in each step (Step 1: T_{1/2} ↓ ↑: 204, 210 K; Step 2: T_{1/2} ↓ ↑: 188, 195 K).

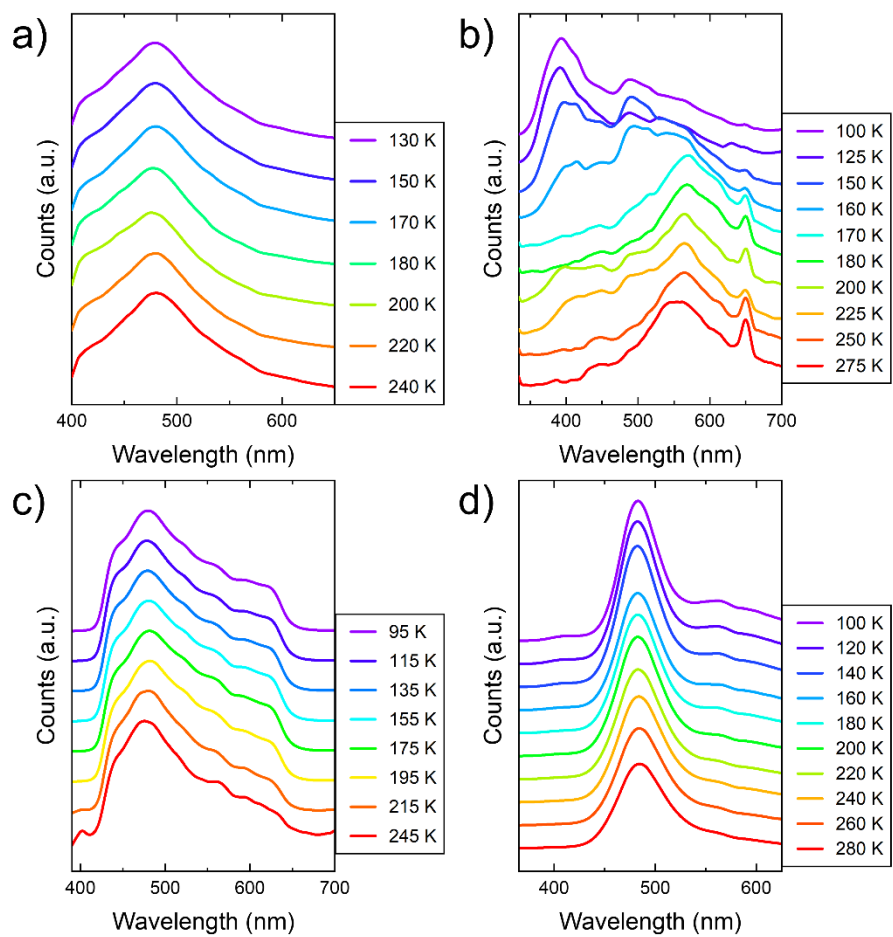


Fig. S5 PL dependence on the temperature for bulk crystals of a) **1**, b) **2**, c) **1·Zn**, and d) **2·Zn**.

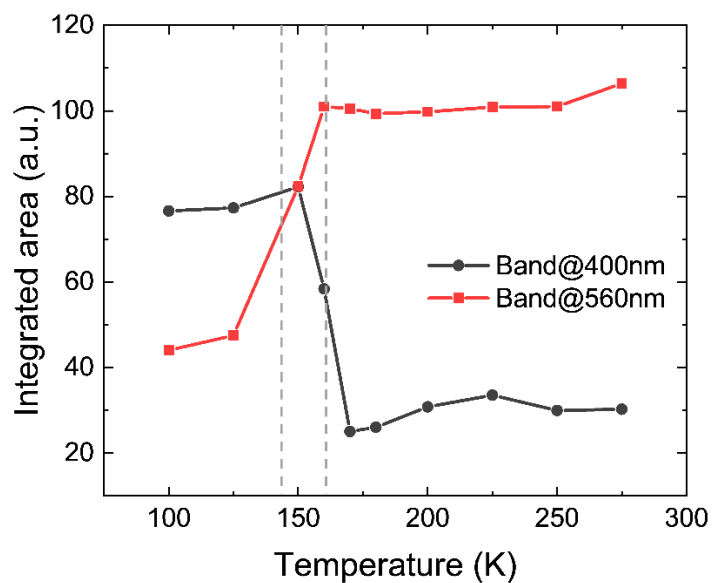


Fig. S6 Dependence of integrated PL intensity (area) vs temperature for the complex **2**. The black scattered line shows the PL area integration from 335 to 465 nm, corresponding to the LS enhanced high-energy band. The red scattered line displays the PL integrated from 500 to 650 nm, corresponding to the enhanced lower energy band at the HS.

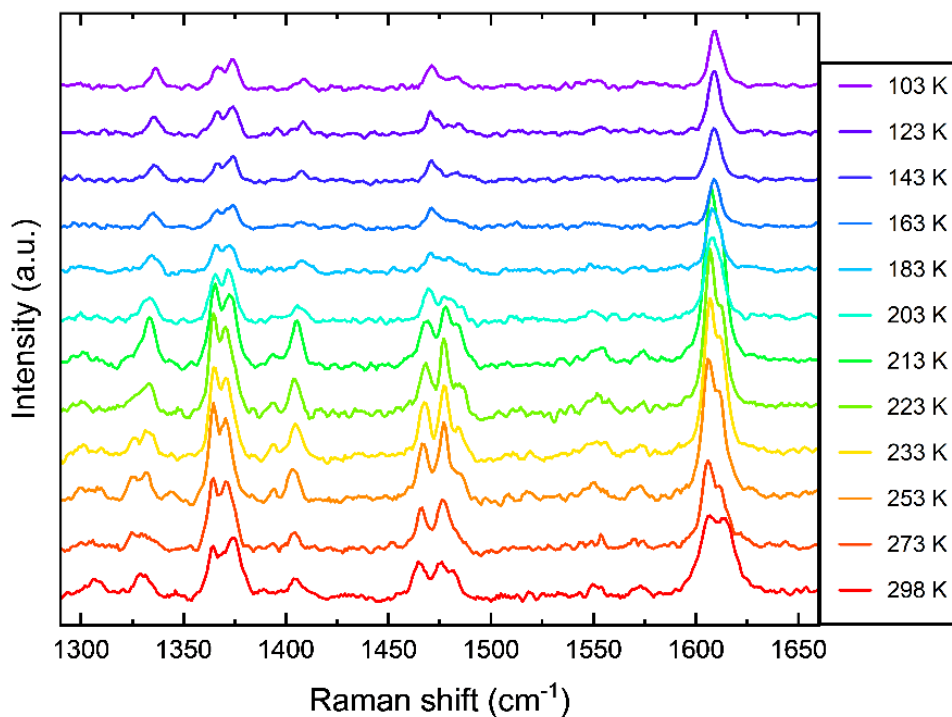


Fig. S7 Stack of temperature-dependent Raman spectra of **1** in bulk in the range between 1290 and 1660 cm^{-1} .

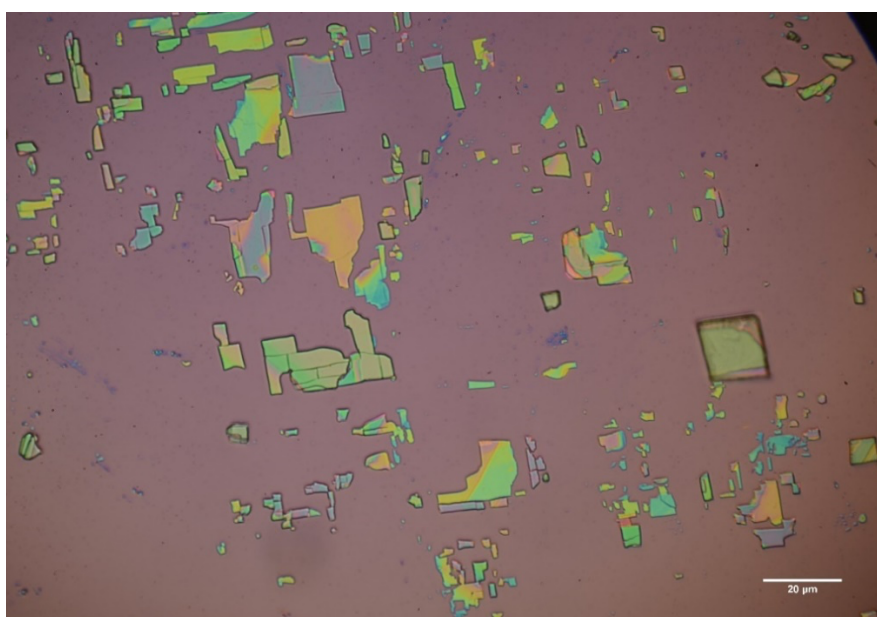
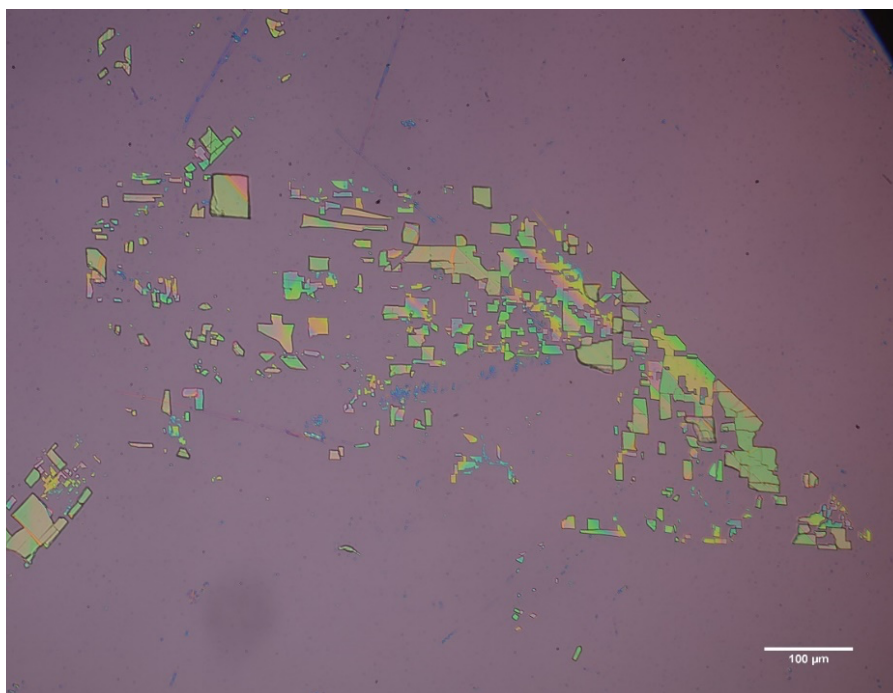


Fig. S8 Example of optical microscopy images of compound **1** after Scotch tape exfoliation.

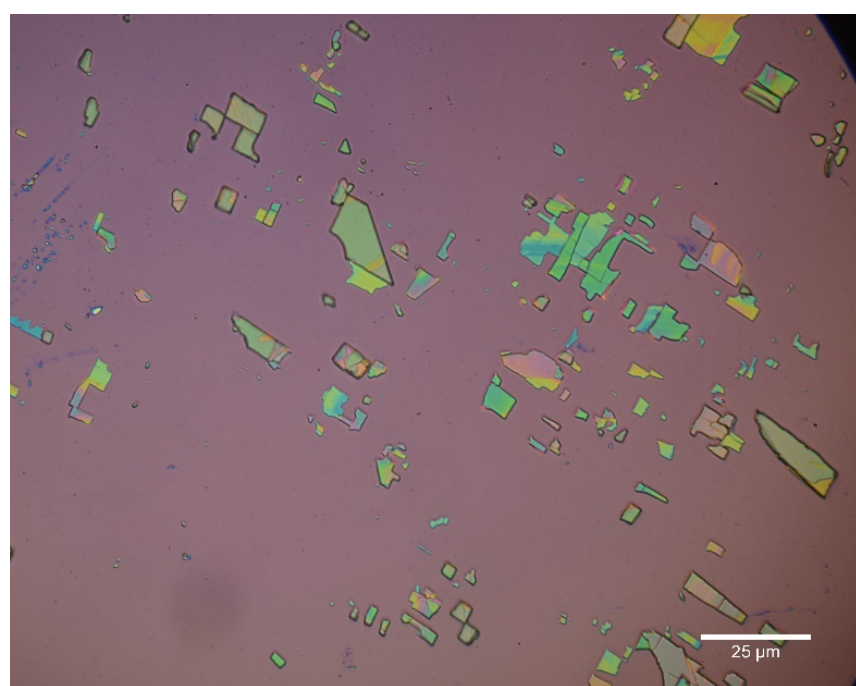
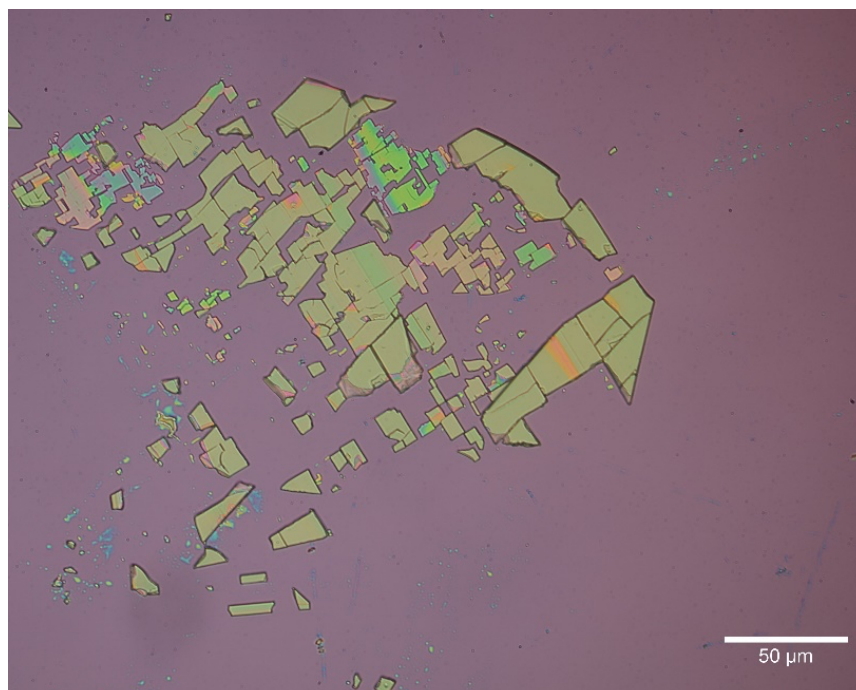


Fig. S9 Example of optical microscopy images of compound **2** after Scotch tape exfoliation.

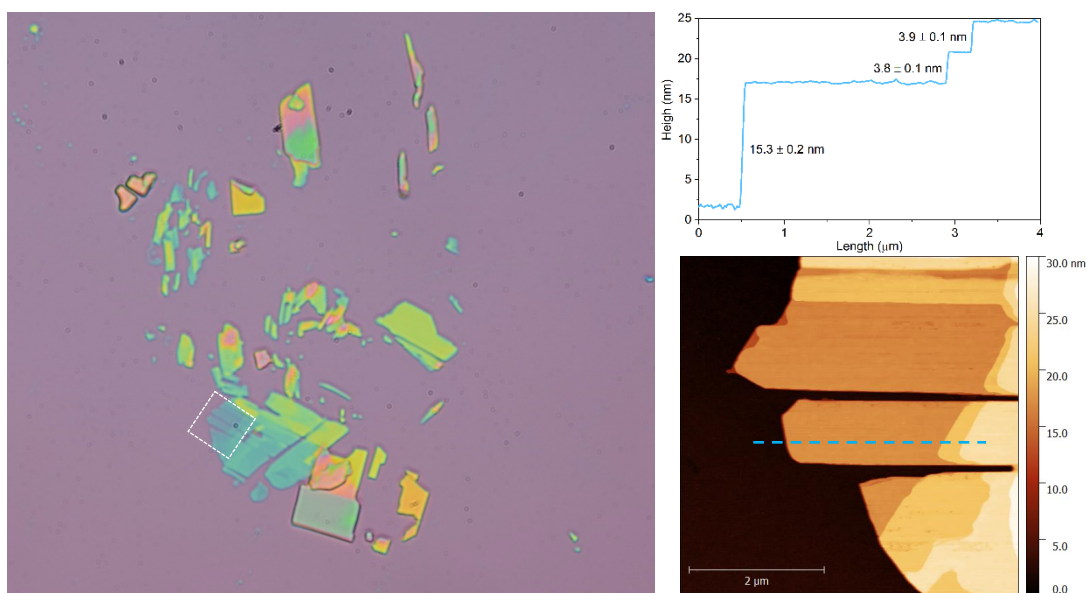


Fig. S10 Optical microscopy and AFM images of **2**. General optical image (left). AFM image (bottom left) of the selected region in dashed white left image with its corresponding height profile (top right; marked in dashed blue in the bottom right image).

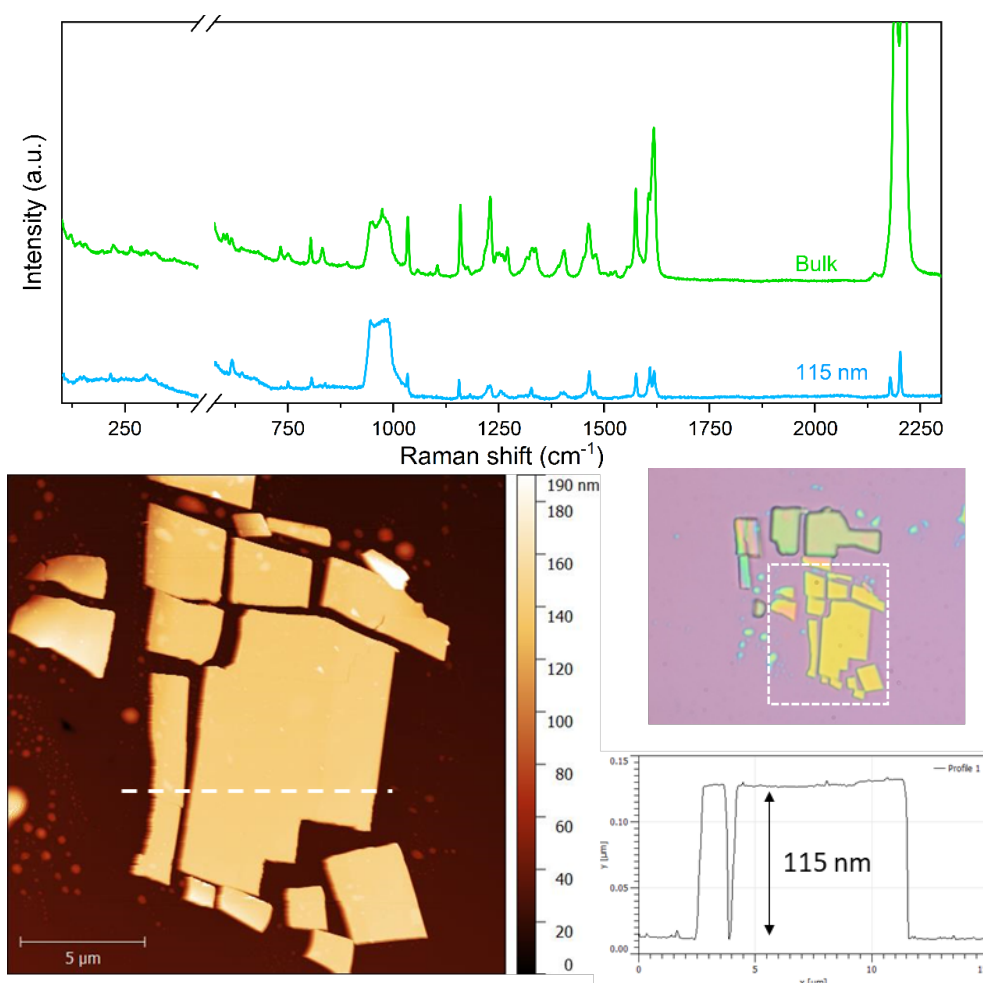


Fig. S11 Raman fingerprints of **2** (green) and an exfoliated flake of 116 nm thickness (blue) in the 200–2300 cm^{-1} range at RT (Top panel). Optical and AFM images of the exfoliated flake of **2** after Raman measurement (Bottom panel). General optical image (medium right). AFM image of the selected region in dashed white in the medium right image (bottom left) and its height profile (bottom right; marked in dashed line in the bottom left image).

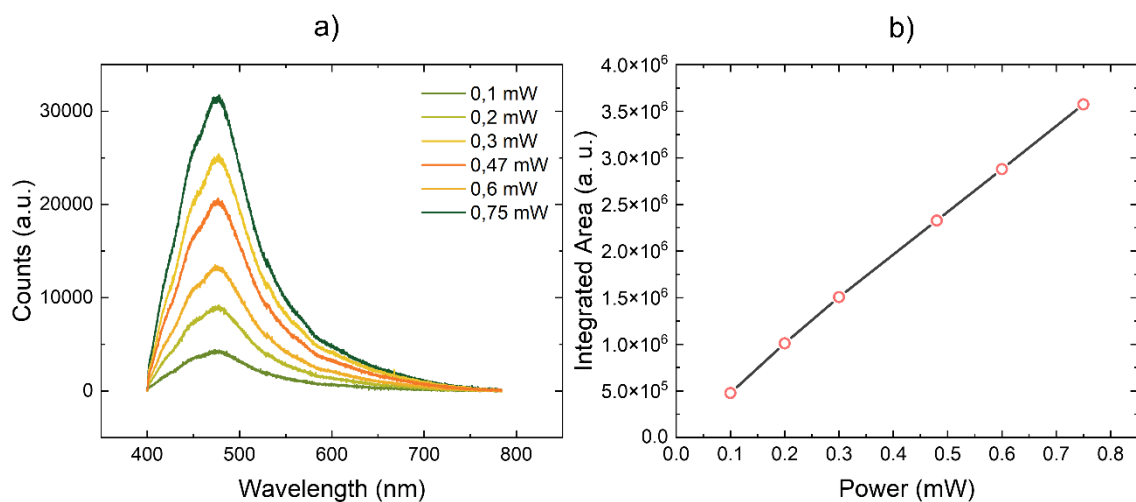


Fig. S12 PL power dependence of a bulk crystal of **1** at room temperature. a) Recorded spectra at the different 375 nm excitation powers. b) Result of the Integrated Area of the PL band for the different powers measured in a).

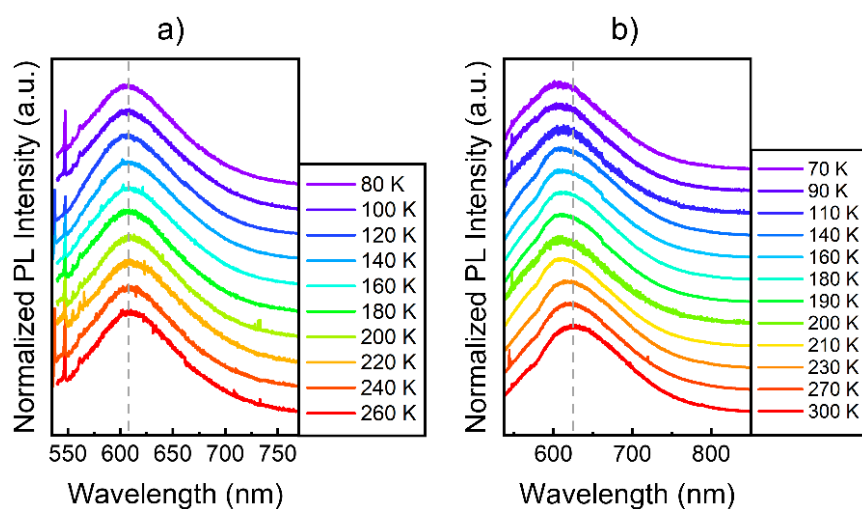


Fig. S13 Resonant PL dependence on the temperature for a) **2** and b) **1** exfoliated flakes. A grey dashed line has been added for reference to the eye.

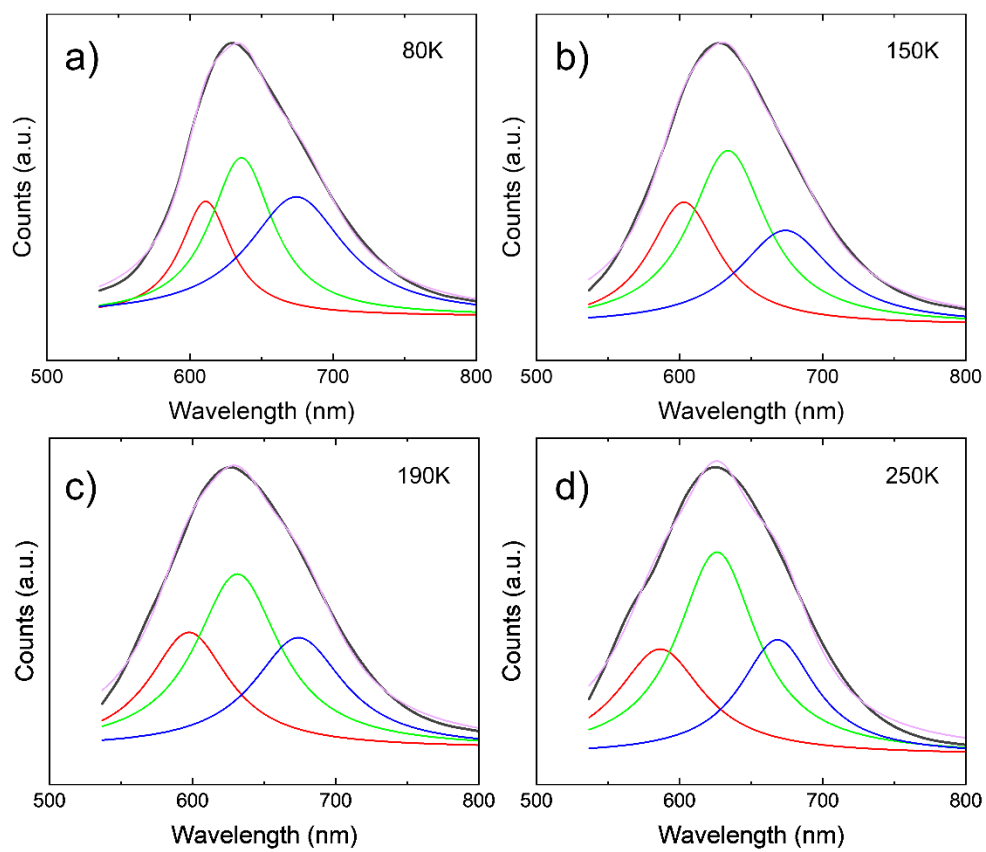


Fig. S14 PL Lorentzian peak deconvolution at different temperatures of an exfoliated sample of **1**. Representative temperatures below and above the SCO transition have been chosen.

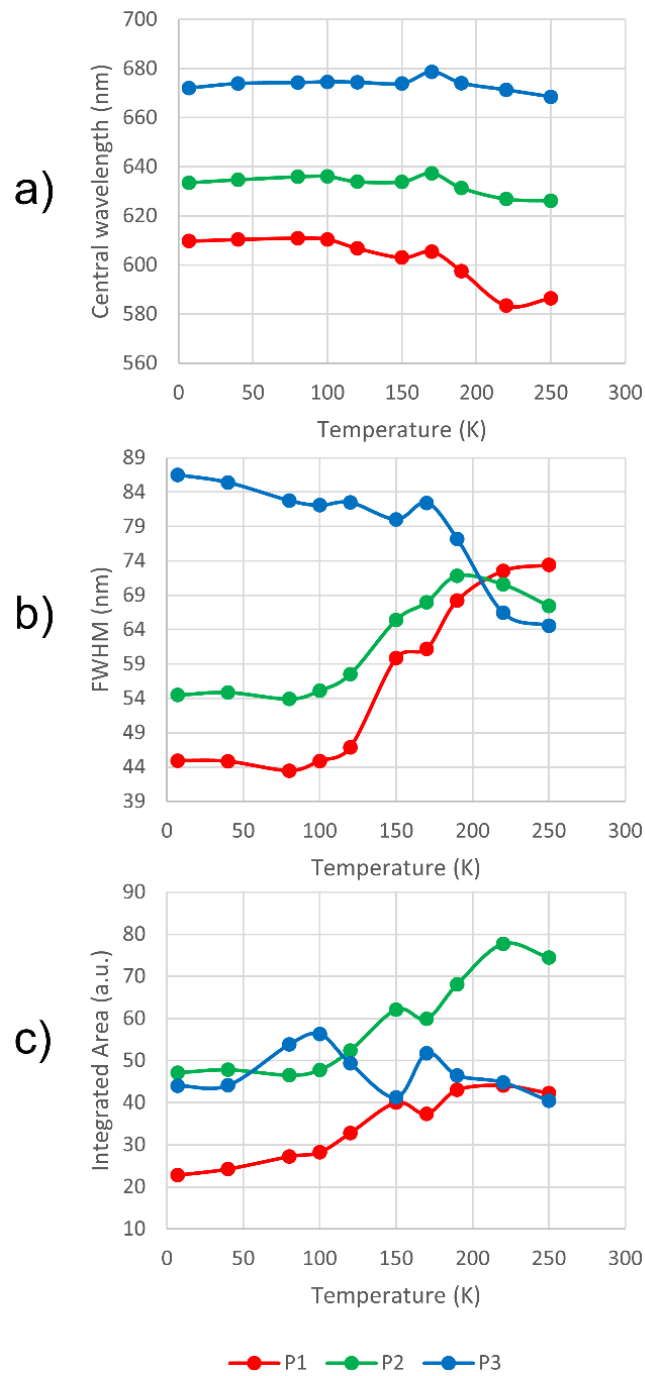


Fig. S15 Results of the Lorentzian peak deconvolution for the exfoliated sample of 1. a) Displays the Central wavelength, b) the FWHM and c) the Integrated Area of the 3 Lorentzian peaks deconvolution the PL spectra shown in **Fig. S11**.

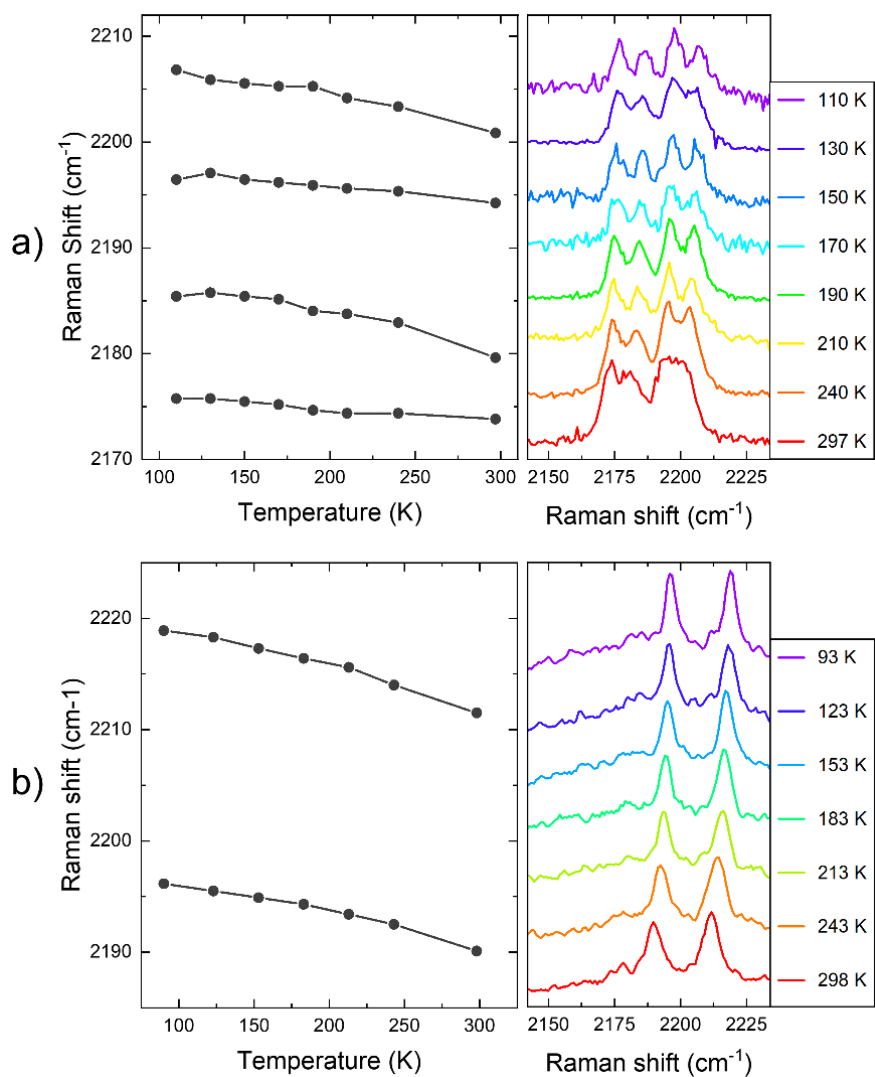


Fig. S16 Raman shift of the CN vibration with the temperature of a) **2** flakes, and b) bulk **1·Zn**. The plot at the left represents the central frequency of the identified Raman vibrational bands. The stack of Raman spectra is shown at the right, which y-axis accounts for intensity in arbitrary units.

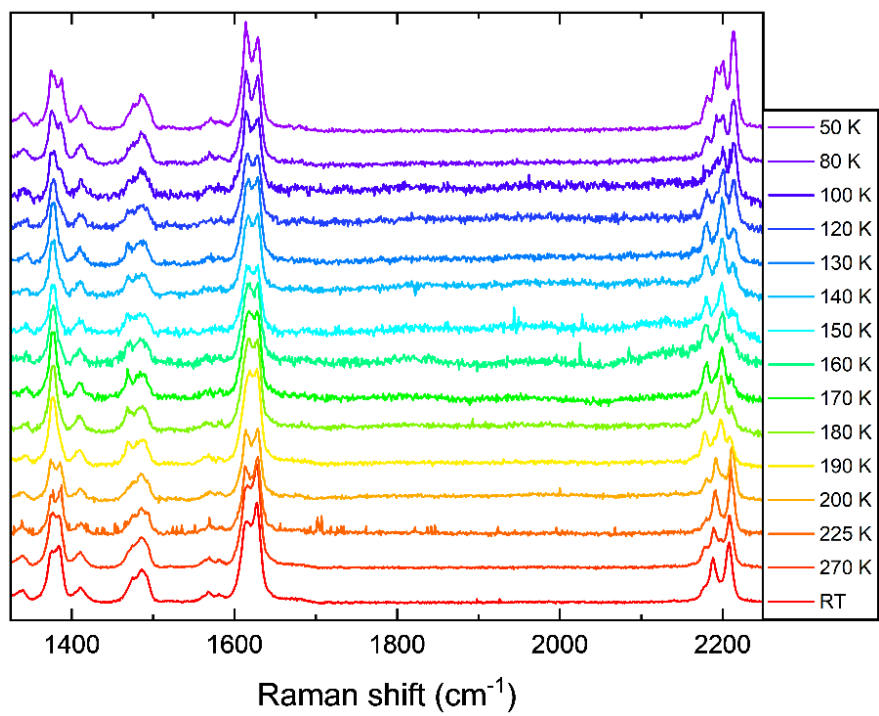


Fig. S17 Stack of temperature-dependent Raman spectra of **1** flakes in the 1350.2220 cm^{-1} range.